



# Femtoscopic $p\Lambda$ Correlations in Pb-Pb Collisions at $\sqrt{s_{NN}} = 2.76$ TeV with ALICE

Hans Beck\*

Institut für Kernphysik, Goethe-Universität, Frankfurt, Germany  
for the ALICE Collaboration

August 14, 2019

## Abstract

Two-particle correlations at small relative momenta give insight into the size of the emitting source. Of particular interest is the test of hydrodynamic models which predict a universal, apparent decrease of the extent of the system with increasing transverse mass  $m_T$  as a consequence of the strong radial flow in heavy-ion collisions at LHC energies. This contribution presents a study of correlations for protons and  $\Lambda$  particles in Pb-Pb collisions at  $\sqrt{s_{NN}} = 2.76$  TeV measured with ALICE. The investigated particle species expand the experimental reach in  $m_T$  due to their high rest mass. Residual impurities in the samples from misidentification and contributions from feed-down are corrected using data-driven techniques. Correlation functions are obtained in several centrality classes and  $m_T$  intervals at large  $m_T$  and show the expected decrease in volume of the strongly interacting fireball for more peripheral collisions. We observe the decrease of the source size with  $m_T$ , predicted by hydrodynamical calculations, out to  $\langle m_T \rangle = 2.18$  GeV/ $c^2$ .

---

\*email: Hans.Beck@cern.ch

# 1 Introduction

Femtoscopy aims at measuring the size of the particle emitting source. Experimentally, this is achieved by studying two-particle correlations at small relative momenta. If the size of the system is large, the emissions of the two particles will likely be substantially separated in space. Therefore, no interaction or symmetrization will take place and the momenta will be uncorrelated. If – on the other hand – the extent of the source is small, the vicinity of the emanation points will trigger the species-specific interplay with a characteristic dependence of the correlation on the momentum difference. Given that the two-particle interaction is known, a source size can be inferred from the correlation function.

No Coulomb or quantum-statistical effects take place in the p $\Lambda$  system and the strong interaction parameters are sufficiently well known from, e. g., bubble chamber experiments. A typical reaction for studying the p $\Lambda$  final-state interaction is the production of  $\Lambda$  baryons by shooting a beam of negatively charged kaons on a hydrogen target as done with the Saclay bubble chamber [1]. The  $\Lambda$  hyperon – created via  $K^- + p \rightarrow \Lambda + \pi^0$  – can subsequently scatter elastically off another proton. Measuring the cross-section of the elastic process differentially vs. the excess energy directly quantifies the attractive final-state strong interaction, which turns out to be comparable to the nucleon-nucleon one.

Based on the model by Lednický and Lyuboshits [2], the sensitivity of the p $\Lambda$  correlation function to the volume of the hot and dense medium created in heavy-ion collisions was first explored in [3]. The correlation was found to be affected in height and shape by the size of the source. Furthermore, the interdependence of the two momenta was shown to keep its susceptibility to a change in source size for radii larger than 4 fm – an advantage over the Coulomb-depleted proton-proton correlations.

A particularly interesting subject is the investigation of the reaction dynamics of the strongly interacting matter generated in Pb-Pb collisions. The large pressure gradients give rise to an expansion of the medium. The resulting collective velocity competes with the thermal velocity  $\sqrt{T/m_T}$ ; consequently the  $m_T$  dependence of the radii probes the dynamics of the source. At low  $m_T$ , no strong collective motion is present and the particles will be correlated over the full extent of the source. At high  $m_T$  in contrast, the radial flow introduces a positive correlation between the emission point and the particle's momentum. Looking only at pairs of particles with a small momentum difference, the couple's constituents will originate from the same region, which is smaller than the geometrical size of the fireball, leading to the apparent shrinking of the particle source with  $m_T$ . To probe the high  $m_T$  regime, it is experimentally beneficial to investigate particles with a high rest mass. So far, the p $\Lambda$  system is the heaviest studied system [4–6].

## 2 Particle Selection

The analyzed Pb-Pb data was taken with ALICE [7]. The T0 and V0 scintillator arrays provided an event-trigger signal and an estimate for the collision centrality. The main detectors for particle tracking in ALICE are the Inner Tracking System, Time Projection Chamber (TPC), and Transition Radiation Detector. Particle identification for this analysis was performed by the TPC and the Time Of Flight (TOF) detector. The vanishing  $\mu_B$  at the LHC entails that matter and anti-matter are produced in equal abundance. While the correlation functions for pairs of  $p\Lambda$  and  $\bar{p}\bar{\Lambda}$  were obtained separately, the selections for particles discussed in the following hold true for their charge conjugates as well.

The proton selection depended on the reconstructed momentum and used the TPC and/or TOF. The resolution of the truncated specific energy loss measurement ( $dE/dx$ ) can be parametrized with a Gaussian of width  $\sigma$ . The TPC provided a separation of the most probable  $dE/dx$  measurement for protons to the one of any other species of more than four  $\sigma$  up to  $p = 0.75$  GeV/ $c$ . Above this kinematic restriction, the expected  $dE/dx$  for protons and the ultra-relativistic electrons becomes too similar, which impeded an unambiguous particle identification by the TPC alone. For higher momenta up to  $p = 5.0$  GeV/ $c$ , TOF allowed for an unambiguous proton identification [8]. With the chosen criteria a proton purity – defined as the number of protons over the number of all selected particles including misidentified tracks – above 99% was achieved over the full dynamic span.

The  $\Lambda$  selection was based upon a  $V^0$  topology finder, which reconstructs the charged decay  $\Lambda \rightarrow p + \pi^-$ ; the hyperon is identified via the invariant mass. Fig. 1 (left) shows a fit to the invariant mass distribution of all  $\Lambda$  candidates employing a Monte-Carlo template for the signal shape in an exemplary phase-space bin with a high yield, namely  $0.5 < |y| < 0.6$  and  $1.0 \leq p_T$  (GeV/ $c$ )  $< 1.5$ , for the 10% most central events. The parametrization allows to determine the purity of the sample – defined as the ratio of picked  $\Lambda$  particles to all taken  $V^0$  vertices – which amounts in this case to  $\text{pur}_\Lambda = 91\%$  within the window in invariant mass of  $\pm 4$  MeV around the PDG value. Determining the purity enables one to correct the correlation function for the uncorrelated background in a following step. Fig. 1 (right) shows the evolution of the  $\Lambda$  purity as a function of rapidity and transverse momentum for the 10% most central events. Protons knocked-out from an interaction with the detector material resemble displaced tracks from weak particle decay vertices. A contribution of protons from material manifests itself in a degradation of the purity for  $p_T < 0.5$  GeV/ $c$ ; the effect is absent for the case of  $\bar{\Lambda}$ . For higher transverse momenta, the purity is 81% for  $|y| > 1.0$ , within  $|\eta| < 0.9$  it is better than 90%.

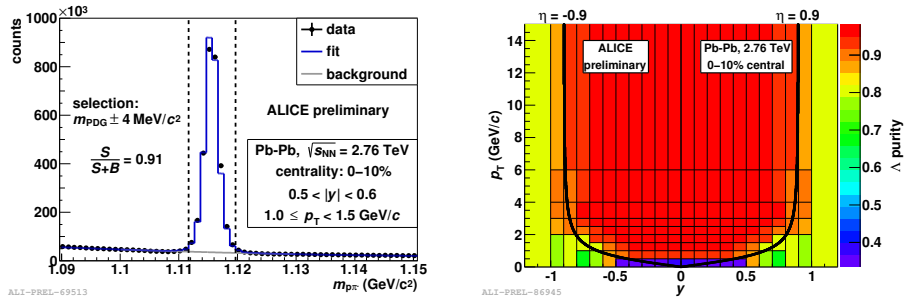


Figure 1: Left: Invariant mass spectrum of  $\Lambda$  candidates in an exemplary phase-bin with a fit using a Monte-Carlo template for the signal shape. Right:  $\Lambda$  purity as a function of rapidity and transverse momentum for the 10% most central events.

### 3 Feed-Down Determination

The  $p\Lambda$  strong interaction is limited in its range to a few fm. Hence, any product from electro-magnetic or weak decays will not contribute to the excess seen at small relative momenta. The contamination in the proton sample mostly stems from the decay  $\Lambda \rightarrow p_{\text{dec}}\pi^-$ . Since no significant  $\Lambda\Lambda$  correlation was seen by the STAR Collaboration [9], the decay proton will also not carry any residual correlation [10–12] from the mother particle.<sup>1</sup> The determination of the amount of this uncorrelated feed-down allows for a correction of the  $p\Lambda$  correlation function with the feed-down fraction  $f_p = \frac{\text{non-primary}}{\text{all}}$ . The outstanding performance of ALICE allows to determine this feed-down fraction in the proton sample directly from the data via the distance of closest approach (DCA) of the track extrapolation to the primary vertex. The two-dimensional (transverse and longitudinal) DCA distribution was obtained differentially in rapidity, transverse momentum, and centrality for the data, as well as for templates from Monte-Carlo simulations for primary protons<sup>2</sup>, protons from weak decays, and protons from an interaction with the detector material. The distinct shapes of the templates – almost flat in DCA for the material contribution, wide for the weak decays, and peaked for the primaries – allow to disentangle the different origins of the charged nucleons by fitting the templates to the data, as pictured in Fig. 2 (left). Selecting only tracks with a DCA smaller than 1 mm in the transverse and smaller than 1.5 mm in the longitudinal direction enhances the primaries in the sample. In the exemplary phase-space bin  $0.0 \leq y < 0.25$  and  $1.0 \leq p_T \text{ (GeV/c)} < 1.5$ , the feed-down fraction  $f_p$  totals to 15%. This arises from the amount of particles which are from weak decays and from material of 15% and less than 1%, respectively.

<sup>1</sup>Recent data from ALICE [13] and STAR [14] suggest a slight  $\Lambda\Lambda$  anti-correlation. The momentum released in the  $\Lambda$  decay will wash this correlation out; the small fraction of  $p_{\text{dec}}\Lambda$  pairs in the  $p\Lambda$  sample will make it a tiny, likely negligible, correction.

<sup>2</sup>According to the common ALICE definition, primary protons include decay products, except products from weak decays of strange hadrons.

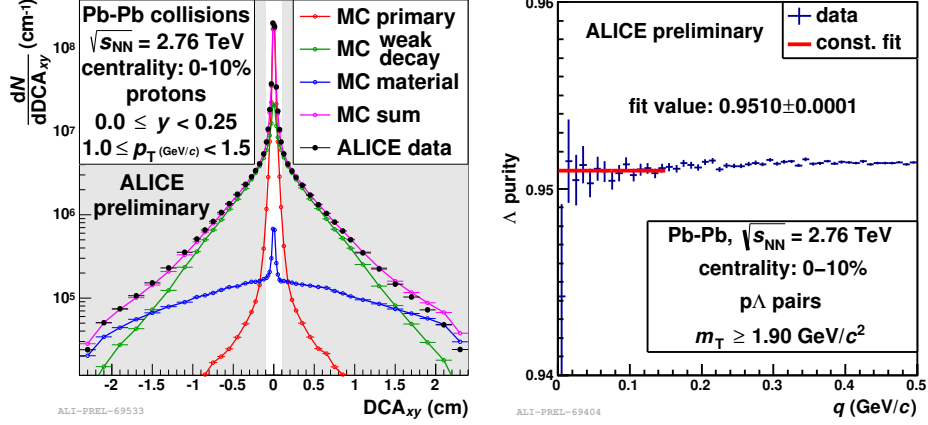


Figure 2: Left: Distribution of the transverse distance of closest of approach of protons to the primary vertex in data with a fit utilizing Monte-Carlo templates in an exemplary phase-space bin. Right:  $\Lambda$  pair purity for pairs with  $m_T \geq 1.9$  GeV/c for the 10% most central events with a constant fit in the region  $0.0 \leq q$  (GeV/c) < 0.15.

Also the  $\Lambda$  sample is contaminated by feed-down. The contributing, dominating weak decays are  $\Xi^0 \rightarrow \Lambda\pi^0$  (BR 99.5%),  $\Xi^- \rightarrow \Lambda\pi^-$  (BR 99.9%),  $\Omega^- \rightarrow \Lambda K^-$  (BR 67.8%), and  $\Omega^- \rightarrow \Xi(\rightarrow \Lambda\pi)\pi$  (BR 32.2%). The reconstruction efficiencies with the chosen  $\Lambda$  selection criteria in this analysis for all  $Y = \Xi^0, \Xi^-, \Xi^+, \Omega^-, \bar{\Xi}^0, \bar{\Xi}^-, \bar{\Xi}^+, \bar{\Omega}^-$  were obtained three-dimensionally in  $p_T^Y \rightarrow (p_T^\Lambda, y^\Lambda)$  for each centrality class of [15] from a Monte-Carlo simulation. Using the  $p_T$ -differential spectra of  $\Xi^-, \bar{\Xi}^+, \Omega^-, \bar{\Omega}^+$  measured by ALICE [15] for several centrality classes and assuming isospin symmetry for the unmeasured  $\Xi^0$  and  $\bar{\Xi}^0$ , enabled us to determine the fraction of  $\Lambda$  hyperons from weak decays.

The  $c\tau = 22$  pm of the electro-magnetic decay  $\Sigma^0 \rightarrow \Lambda\gamma$  (BR 100%) is much larger than the range of the strong interaction, but also too small to be resolved experimentally. In [16] it was found that the final-state interaction in the  $p\Sigma^0$  channel is much smaller than in the  $p\Lambda$  system. Thus, a significant fraction of  $\Lambda$  come from  $\Sigma^0$  and are uncorrelated with primary protons. We use the fraction of  $\Lambda$  from  $\Sigma^0$  – properly taking into account all strongly decaying resonances – from the thermal model of [17], while systematically considering the study in [18] with an additional variation in the freeze-out temperature, and the results of [19] with the value at the kinetic and chemical freeze-out. All models give that about 30% of the  $\Lambda$  originate from a electromagnetic decay. We unite the fraction from weak and electromagnetic hyperon decays in the feed-down fraction  $f_\Lambda$ .

## 4 Corrections and Results

The raw  $p\Lambda$  correlation as a function of the momentum difference is obtained as the ratio of pairs from real events over those reconstructed from mixed events for three centrality divisions and up to four  $m_T$  classes for each centrality class. Dealing with non-identical particles, we use the generalized momentum difference introduced in [20] by R. Lednický  $\tilde{q} = |q - P(qP)/P^2|$ ,  $q = p_1 - p_2$ ,  $P = p_1 + p_2$ , where  $p_1$  and  $p_2$  are the momenta of the particles. In the following, we omit the tilde. The overall pair purity factorizes:  $\text{pur}(q, m_T) = \text{pur}_\Lambda(q, m_T) \cdot (1 - f_p(q, m_T)) \cdot (1 - f_\Lambda(q, m_T))$ . The  $\Lambda$  pair purity  $\text{pur}_\Lambda(q, m_T)$  is shown exemplary in Fig. 2 (right) for the 10% most central events and the highest  $m_T$  class,  $m_T \geq 1.9 \text{ GeV}/c^2$ . Its value of 95.1% is constant over the region of interest  $q < 0.15 \text{ (GeV}/c)$  and beyond. It is obtained by looking up the single-particle  $\Lambda$  purity in the  $(y, p_T)$ -differential histograms for the given centrality; the same holds for  $f_p$  and  $f_\Lambda$  accordingly. All impurities constitute – as discussed – an uncorrelated background. Hence, the corrected correlation function can be attained by scaling the raw correlation function with the inverse pair purity:

$$C_2^{\text{corr.}}(q, m_T) = \left( \frac{1}{\text{pur}(q, m_T)} \cdot (C_2^{\text{raw}}(q, m_T) - 1) \right) + 1. \quad (1)$$

The effect of the finite momentum resolution was studied with a Monte-Carlo simulation. For small relative momenta, i. e.  $(q_{\text{rec}} + q_{\text{gen}})/2 \leq 0.1 \text{ GeV}/c$ , where  $q_{\text{rec}}$  is the reconstructed and  $q_{\text{gen}}$  is the generated relative momentum, the deviation, quantified as  $(q_{\text{rec}} - q_{\text{gen}})/\sqrt{2}$ , can be parametrized with a Gaussian with a mean of  $-0.32 \pm 0.02$  and  $-0.38 \pm 0.08 \text{ MeV}/c$  and a width of  $7.26 \pm 0.02$  and  $7.13 \pm 0.07 \text{ MeV}/c$  for the 0–10 and 30–50% most central events. In an  $m_T$ -differential study, the width turned out to slightly increase by less than  $2 \text{ MeV}/c$  for higher  $m_T$ .

Fig. 3 shows a set of exemplary correlation functions corrected via Eq. 1, i. e. remedied for the uncorrelated background coming from weak and electromagnetic decays. The correlation functions for pairs of particles and pairs of anti-particles were merged following the recipe of the Particle Data Group [21]. The systematic errors include a variation of the correction for the electromagnetic feed-down, a change in the hyperon input spectra for the correction of the  $\Lambda$  from weak decays, an altered momentum resolution, normalization, invariant mass selection of the  $\Lambda$ , changed DCA cuts on the proton, a varied two-track resolution cut, and dominantly the uncertainty on the  $p\Lambda$  interaction when fitting the data. The top panel shows the centrality dependence, i. e. the 0–10% most central events in red and the 30–50% most central events in blue; both samples have a mean transverse mass of  $1.5 \text{ GeV}/c^2$ . One clearly sees the expected effect of an increased width and height of the excess at small relative momenta, which translates into a smaller source size, for the more peripheral collisions. The bottom panel shows the dependence on  $m_T$  with the green points representing  $1.0 \leq m_T \text{ (GeV}/c^2) < 1.4$  resulting in  $\langle m_T \rangle = 1.27 \text{ GeV}/c^2$  and the orange symbols depicting  $m_T \geq 1.9 \text{ GeV}/c^2$  yielding  $\langle m_T \rangle = 2.18 \text{ GeV}/c^2$

for the 0–10% most central events. Also here, a clear ordering is apparent with the higher  $m_T$  giving evidence for a smaller source than at lower  $m_T$ , matching the expectation within the hydrodynamic picture outlined in the introduction. Note that the correlation function with  $\langle m_T \rangle = 2.18 \text{ GeV}/c^2$  exceeds the  $\langle m_T \rangle$  of any previous measurement from [6] at the SPS, [5] at RHIC or [22,23] at the LHC.

## 5 Summary

The supreme performance of ALICE makes it possible to collect very pure samples of protons and  $\Lambda$  with rich statistics. We obtained  $p\Lambda$  correlation functions multi-differentially in centrality and transverse mass. They were corrected for misidentification and contamination from weak and electromagnetic decays, employing data-driven methods to quantify the impurities. The correlation functions presented here represent the largest  $m_T$  reach of any femtosopic measurement, with result being shown for  $m_T \geq 1.9 \text{ GeV}/c^2$ . The conveyed centrality dependence of the  $p\Lambda$  correlations exhibits the expected behavior of a smaller source for more peripheral collisions. The communicated  $m_T$ -differential correlations, spanning a range in  $\langle m_T \rangle$  of more than  $0.9 \text{ GeV}/c^2$ , display the decrease in source size with  $m_T$ , qualitatively agreeing with hydrodynamic predictions, out to highest  $\langle m_T \rangle = 2.18 \text{ GeV}/c^2$ .

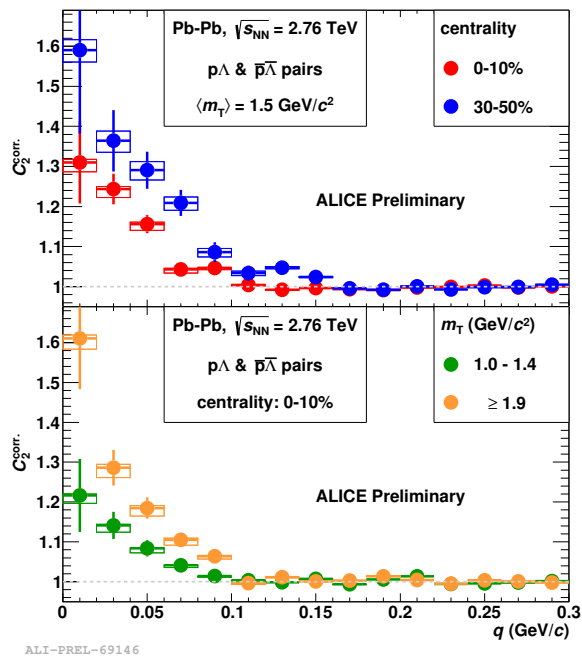


Figure 3: Exemplary  $p\Lambda$  and  $p\bar{\Lambda}$  correlation function corrected for weak and electromagnetic decays. Centrality dependence at the top,  $m_T$  dependence at the bottom.

## References

- [1] B. Sechi-Zorn, B. Kehoe, J. Twitty, and R.A. Burnstein, Phys. Rev. **175**, 1735 (1968)

- [2] R. Lednický and V.L. Lyuboshits, *Sov. J. Nucl. Phys.* **35**, 770 (1982)
- [3] F. Wang and S. Pratt, *Phys. Rev. Lett.* **83**, 3138 (1999)
- [4] J. Adams *et al.* (STAR Collaboration), *Phys. Rev. C* **74**, 064906 (2006)
- [5] H.P. Gos for the STAR Collaboration, *Eur. Phys. J. C* **49**, 75 (2007)
- [6] T. Anticic *et al.* (NA49 Collaboration), *Phys. Rev. C* **83**, 054906 (2011)
- [7] The ALICE Collaboration, *JINST* **3**, S08002 (2008)
- [8] The ALICE Collaboration, *Int. J. Mod. Phys. A* **29**, 1430044 (2014)
- [9] N. Shah for the STAR Collaboration, *Nucl. Phys. A* **914**, 410 (2013)
- [10] F. Wang, *Phys. Rev. C* **60**, 067901 (1999)
- [11] V.M. Shapoval, B. Erasmus, R. Lednický, and Yu.M. Sinyukov, arXiv:1405.3594 [nucl-th]
- [12] A. Kisiel, H. Zbroszczyk, and M. Szymański, *Phys. Rev. C* **89**, 054916 (2014)
- [13] J. Salzwedel for the ALICE Collaboration, Talk given at WPCF 2014
- [14] The STAR Collaboration, arXiv:1408.4360 [nucl-ex]
- [15] The ALICE Collaboration, *Phys. Lett. B* **27**, 216 (2014)
- [16] P. Kowina *et al.*, *Eur. Phys. J. A* **22**, 293 (2004)
- [17] M. Chojnacki, A. Kisiel, W. Florkowski, and W. Broniowski, arXiv:1102.0273 [nucl-th]
- [18] A. Andronic, P. Braun-Munzinger, and J. Stachel, *Nucl. Phys. A* **772**, 167 (2006)
- [19] F. Becattini, M. Bleicher, J. Steinheimer, and R. Stock, *PoS CPOD 2013*, 010 (2013)
- [20] R. Lednický, arXiv:nucl-th/0112011
- [21] K.A. Olive *et al.* (Particle Data Group), *Chin. Phys. C* **38**, 090001 (2014)
- [22] M.P. Szymański for the ALICE Collaboration, *Nucl. Phys. A* **904-905**, 447c (2013)
- [23] H. Beck for the ALICE Collaboration, *J. Phys.: Conf. Ser.* **446**, 012013 (2013)